Review



# A Review of Various Synthesis Methods of Graphene and Applications

Balaji S *, Madhumidha V , Haritha K , Cyril A

Posted Date: 14 September 2023

doi: 10.20944/preprints202309.0937.v1

Keywords: Graphene Oxide; Reduced Graphene Oxide; 2D-material; hexagonal honeycomb-like structure; sp2 hybridization

*Review*

# A Review of Various Synthesis Methods of Graphene and Applications

**S. Balaji [1,*], V. Madhumidha [1], K. Haritha [1] and A. Cyril [2]**

[1] Research scholar, Alagappa University, Karaikudi
[2] Head of the Department, Raja Doraisingam govt. arts college, Sivagangai
* Correspondence: balajis9384@gmail.com

**Abstract:** Graphene is a two-dimensional carbon atom with a hexagonal honeycomb-like structure in which the sp2 hybridization occurs. GO sheets are highly oxidized and have oxygen-containing groups. Properties of electronics, mechanicals, magnetics, and optics, Oxidized Methods for Brodies, Staudenmaier, Hofmann, Hummers, Improved Hummers, and Tour's Methods Reduction of Graphene oxide methods Chemical Reduction using sodium borohydride, 2,4-dinitrophenylhydrazine, Hydrazine hydrate, Thermal Reduction, Hydrothermal Reduction, Exfoliation Reduction, Catalytic Reduction, and the green synthesis route for reduction, The reduction of graphene oxide has a wide range of applications, including its use in energy storage devices for Solar cells, Supercapacitors, LIG-based sensors, River Water sensors, Battery, hydrovoltaic generators, OLED Screen, and Graphene Shielding. This review will determine the future of a few applications.

**Keywords:** graphene oxide; reduced graphene oxide; 2D-material; hexagonal honeycomb-like structure; sp2 hybridization

## 1. Introduction

The two-dimensional monolayer of carbon atoms known as graphene has a hexagonal honeycomb-like structure, sp2 hybridized carbon bonds, and a p bond that generates a network of decentralized electrons that is both responsible for electron conduction and weakly interacts with other graphene layers or a substrate. In the various techniques that can be utilized for graphene and its derivatives [1,2], The weak van der Waals connections between the layers of graphite allow for mechanical exfoliation to create graphene. The multifunctional graphene-based nanomaterials (GBNs), including graphene oxide (GO) and reduced graphene oxide (rGO), are easily created through various surface modifications and have found extensive usage in a variety of sectors, including physics, medicine, and electronics [37]. To comprehend the timeline of graphene research, graphene as the limit of graphite with the fewest value of layers. In this sense, the extraordinary properties of honeycomb carbon are nothing new. These same qualities have recently made graphite, the more expensive but similarly structured compound hexagonal boron, a promising material for use as a dry lubricant. It has proven to possess numerous desirable qualities, including mechanical strength, electrical conductivity, molecular barrier capabilities, and other outstanding characteristics [36]. Strongly oxidized GO sheets are a distinct group of groups that include oxygen. Properties of electronics[3], mechanicals[4], magnetics[5], and optics[5], Oxidized Methods for Brodies[6], Staudenmaier[7], Hofmann[8], Hummers[9], Improved Hummers[10,11], and Tour's Methods[12,13] Reduction of Graphene oxide methods Chemical Reduction using sodium borohydride[14], 2,4-dinitrophenylhydrazine[15], Hydrazine hydrate[10], Thermal Reduction[16], Hydrothermal Reduction[17], Exfoliation Reduction [18], Catalytic Reduction[15], and the green synthesis route for reduction[19,20]. The morphology and sample appearance of the material are characterized by X-ray diffraction (XRD)[18]. Fourier transform infrared (FTIR) [21], UV-visible [22], energy dispersive X-ray (EDX)[23], X-ray photoelectron spectroscopy (XPS)[24], Raman spectroscopy[10], scanning electron microscopy (SEM), [10] transition electron microscope (TEM)[24], vibrating sample magnetometer (VSM)[25], and

 doi:10.20944/preprints202309.0937.v1



thermogravimetric analysis (TGA)[26], respectively. The reduction of graphene oxide has a wide range of applications, including its use in energy storage devices for Solar cells [27], Supercapacitors [28], LIG-based sensors [29], River Water sensors [30], Batteries[31], hydrovoltaic generators[32], OLED Screen[33], Graphene Shielding[34,35]. This review will determine the future of a few applications. Though there are methods to improve its characteristics, graphene oxide is not a good conductor of electricity. The industrial-scale economic analysis showed that, following execution, the technique would be viable. A use for graphene and its derivatives has been investigated, including energy generation and storage, optical devices, electronic devices, photonic devices, drug delivery, clean energy, and chemical and biosensors. Reduced graphene oxide using a unique synthesis method was developed and described in this research.

## 2. Graphene Property

### *2.1. Electronic Property*

The monolayer Metal oxide is a direct bandgap semiconductor at the K point with a band gap of 1.75 eV, has no noticeable bandgap, and establishes as a metallic character with the p band and p* band crossing at the Dirac point at the hexagonal bend of the graphene's Brillouin zone. The partial density of states can provide in free-standing graphene, the half-filled 2pz orbitals of carbon atoms perpendicular to the planar p band and p* band, which touch at the Dirac point closely at the Fermi energy, corresponding to finding the band energy. For metal oxide, the bottom of the conduction band is dominated by M-4d orbitals, whereas the top of the valence band is M -d and O-p orbitals[3]. In addition, near the top of the valence band, the M-d and O-p orbitals hybridize.

### *2.2. Mechanical Properties*

The most frequently estimated tensile characteristics show a general tendency to decrease extension to break and increase tensile stress as graphene nanoparticle loading increases for all processing conditions. Higher processing speeds are required for the effect to be noticeable in nanocomposites with low filler concentrations. On the other hand, nanocomposites with high graphene nanoparticle loading Tensile characteristics are affected by processing speed, barrel/die set temperature, filler concentration, and workstation type[4]. A sample is repeatedly tape-exfoliated and then transferred to a substrate.

### *2.3. Magnetic Properties*

In this part, we describe the magnetic characteristics of GO sheet precursors and rGO-QDs samples at various reduction temperatures in detail. When an unpaired electron system is to an external magnetic field, the degenerate electron spin state splits with a difference in energy between the two states[5,25]. An absorbed photon's energy obtained from a frequency (ν) of external radiation can cause the unpaired electron spin to flip from lower to upper or upper to lower energy levels.

### *2.4. Optical and Luminescence Properties*

Graphene will be used commercially in optoelectronics in touchscreens, liquid crystal displays (LCDs), and organic light-emitting diodes (OLEDs). 90% of light and have an electrical conductivity than 1 $106^{-1}m^{-1}$. Graphene is an almost transparent substance that can transmit 97.7% of visible light. As previously stated, it is also conductive; therefore, Optoelectronic applications such as touchscreens for smartphones, tablets, televisions, and desktop computers. The characteristic absorption peak for GO appeared at ~230 nm, at the π-π* transition of aromatic $sp^2$ domains. The -conjugation of aromatic $sp^2$ in rGO-QDs increases due to an extended -electron system within the honeycomb-like structure. As the -conjugation increases, less energy is required for the transition, corresponding to the observed shift of the absorption to a longer wavelength[5,41]. Furthermore, the weak absorption peak of rGO-QDs also appears at ~309 nm, which can be the n-π* transition. The carboxyl and carbonyl groups are attached to the surface of rGO-QDs.

 doi:10.20944/preprints202309.0937.v1



## 3. Experimental Synthesis

The many graphene oxide synthesis methods are Brodie's method, Staudemaier's method, Hoffmann's method, Hummer's method, modified Hummers method, and Tour method.

### *3.1. Brodie's Oxidation Method*

The oxidation of the graphite using Brodie´s method of Fuming Nitric acid (200 mL) was added to a flask with a cooling jacket and cooled to 0°C in a cryostat. The graphite powder (10 g) was introduced into the flask and thoroughly dispersed to avoid agglomeration. Next, potassium chlorate (80 g) for 21 h at 0°C is necessary potassium chlorate. Explosions can occur. Once the reaction had finished, the mixture was distilled water and vacuum-filtered until the pH of the filtrate was neutral [6,40]. The produced substance, graphite acid, is in pure water but not in acidic environments. This approach has disadvantages, including a lengthy reaction time and the emission of hazardous gases.

### *3.2. Staudenmaier Method*

The synthesis of GO from 1 g of natural graphite flake mixed with 27 mL of a 2:1 ratio $H_2SO_4$:$HNO_3$ solution in an ice bath, then gradually adding 11 g of $KClO_3$, keeping the reaction's temperature below 35°C, stirred for 96 hours, 800 mL of distilled water added while swirling the mixture, and a 0.45 mm nylon membrane filter is using [7]. The GO precipitate was washed several times in a 5% HCl solution to remove sulfate ions, using the $BaCl_2$ test, and then in distilled water to remove chloride ions, using the $AgNO_3$ test.

### *3.3. Hofmann Method*

Hofmann's synthesis of $H_2SO_4$ (98%) and $HNO_3$ (68%) was added and mixed in an ice bath for 30 minutes. The mixture was then aggressively agitated while graphite (1 g) was added. While the reaction flask was submerged in an ice bath, potassium chlorate (10 g) was slowly added. Once the potassium chlorate is fully dissolved, the reaction flask is loosely closed to allow the gas to escape, and the mixture is continuously stirred at room temperature for 96 hours. They were placed in 300 mL of deionized water[8]. Sulfate ions were removed from graphene oxide by centrifuging and washing with DI water until the negative interfering radical between the chloride and sulfate ions was dissipated. After that, it was dried in a vacuum oven for 12 hours.

### *3.4. Hummer's Method*

The 1 g of graphite and 23 mL of $H_2SO_4$ were stirred at 5°C. After an hour, the temperature raised to 40°C, at which point 3 $KMnO_4$ was added. Drop by drop added 46 mL of deionized water was then added over the course of three hours while maintaining a 90°C temperature adjustment to avoid a rapid temperature rise. It took around 40 minutes to achieve 90°C, and the mixture was stirred for another 30 minutes when the temperature hit 90°C, followed by a 25-mL water addition, then 1mL of $H_2O_2$ was added. The solutions were filtered using a glass fiber filter after another 15 minutes of stirring. Prepare 300 mL of the 10% HCl solution and the graphene oxide particle filtration for the acid dispersion method [9,21,38]. Several times with a glass fiber filter before filtering again, after filtering several times in 300 mL of acetone for total purification. In a vacuum oven dried at 40°C for 72 hours.

### *3.5. Improved Hummers Method*

Graphite using $KMnO_4$ as the oxidizing agent, 180 mL of the con.$H_2SO_4$, and 21 mL of the con. $H_3PO_4$ stirred for 10 minutes. 1.5 g of graphite and 4.5g of $KMnO_4$ were gradually added to the $H_2SO_4$/$H_3PO_4$ mixture; the reaction was the constant stirring at 50°C for 12 h. The mixture was placed in an ice bath, followed by 1.5 mL of $H_2O_2$ to stop the process. They are washed several times through vacuum filtration with deionized water, HCl, and ethanol [10,11,38]. Finally, the slurry with dry diethyl ether was added and dried at 100°C for 12 hours.

Preprints (www.preprints.org) | NOT PEER-REVIEWED | Posted: 14 September 2023 doi:10.20944/preprints202309.0937.v1



*3.6. Tour Method*

The synthesis of GO has been Tour's approach. Graphite powder by soaking it for seven days in a solution of strong sulfuric acid and nitric acid (1:1 volume ratio). A solid mixture of 1 g of acid-saturated graphite and 4 g of $KMnO_4$ (1:4 weight ratio), held in an ice bath, was slowly and progressively added to a cooled mixture of 70 mL of concentrated sulfuric acid and 10 mL of phosphoric acid (7:1 volume ratio) continuously stirred in room temperature. The solution changes to a reddish-brown color. Then the solution was heated for 15 hours at 50°C. After that, an ice bath addition of 1 mL of $H_2O_2$[12,13,40]. A solution change from a light brown or yellow color. After adding water to the solution and stirring for a few hours. Then washed with water, HCl, and ethanol and dried at 55°C for 12 hours in a hot air oven.

**4. Reduction of Graphene Oxide**

*4.1. Chemical Reduction of Graphene Oxide*

The 12.5 mL GO solution was diluted with DI water to 1.0 mg/mL under ultrasonication. Then $NaBH_4$ was dissolved in 1.2g of a 50 mL NaOH solution (pH = 9). The $NaBH_4$-NaOH solution was then slowly added to the GO solution. The heated solution at 80°C in an oil bath and stirred for 1 hour [14]. They were washed multiple times with water and ethanol before being vacuum dried for 12 hours. The reduction of graphene oxide with DNPH took 100 mg of graphene oxide mixed in 100 mL of distilled water using an ultrasonic for 1 hour. They adjusted to pH 8 for 1 M NaOH. Then 2,4-dinitrophenylhydrazine salt (1 g) was added and stirred for 2 hours at 80°C [15]. Afterward, the solution was filtered using Whatman No. 1 filter paper, washed with ethanol, acetone, and a mixture of acetonitrile and water, then dried for 24 hours at 70 °C. 2 g of GO and 650 mL of water are added, then stirred for 30 minutes [10,39]. Then oil bath and 0.65 mL of hydrazine hydrate were added and then heated to 80°C with a continued stirrer for 72 hours. The solution is washed several times with water and then centrifuged for 10 minutes at 8000 rpm and dried for 24 hours at 80°C.

*4.2. Thermal Reduction of GO*

The dried brown powder was known as graphene oxide (GO)[16]. A mixture of GO 200 mg and 200 mL of the aqua test was ultrasonication for 3 hours to exfoliate graphene sheets in GO powder. The mixture was condensed and vacuum dried for 72 hours to form a dark brown powder. GO powder was reduced by annealing at 400°C. The dark brown powder was changed to a dark powder after thermal treatment as rGO powder. The rGO was extracted from GO by thermal reduction. GO has a reduced temperature (300 °C). A sudden change in temperature causes the elimination of functional groups and oxygen atoms from carbon planes, and exfoliation of GO takes place to produce rGO. The rGO can be considered chemically derived graphene, whose structure is from one layer to multi-layers. rGO hydrothermally synthesized using 800 mg GO nanosheets incorporated with 100 mg Ag in 80 ml deionized water under vigorous stirring for 20 min [17]. The solution was then centrifuged for 30 min, transferred to a 100-ml Teflon-lined autoclave, sealed, and heated at 200°C for 24 h. The final product was washed and dried at 200 °C.

*4.3. Exfoliated Reduction*

Aqueous colloids of XGO were made by ultrasonically dissolving 0.25g of GO in 125 mL of distilled water and centrifuging for 2 hours to remove any unexfoliated GO [18]. The XGO dried at 90°C for 12 hours. Then RGO was prepared by dissolving 100 mg of XGO into 200 mL of distilled water, stirring at 95°C for 96 hours, and drying in a vacuum oven for 24 hours.

*4.4. Catalytic Reduction*

4.8 mL of 4-NPH (10 ppm) or RhB (7.5 ppm) aqueous solution and 1.0 mL of NaBH4 (0.75 M) into a 10-mm path-length quartz cuvette (6 mL) containing 0.1 mL of GO/Ag nanoparticle suspension

Preprints (www.preprints.org) | NOT PEER-REVIEWED | Posted: 14 September 2023 doi:10.20944/preprints202309.0937.v1



(5 mg/mL) to do this process [15]. For the catalyst recycling test, the RGO/Ag nanoparticles were separated and filtered after the reaction, cleaned, and put at 65°C for utilization in the runs.

*4.5. Green Synthesis Route for Reduced GO*

GO dispersion with a concentration of 2 mg/mL was prepared by dispersing 100 mg of GO in 50 mL of DI Water using ultrasonication for 30 min. 50 mL of GO, then the mixture was stirred and heated at 80°C for 3 hours [19,20]. The brownish color converted to a black solution. The obtained solutions were centrifuged at 5,000 rpm and then washed several times with DI water and ethanol. Furthermore, the product dried at 60°C for 12 hours.

## 5. Characterization

The Characterization of graphene used in spectroscopy techniques is XRD, FTIR, UV-Visible, EDX, XPS, and Raman, then Microscopy techniques are SEM, TEM, and other techniques are VSM, DGA, and Density.

*5.1. X-ray Diffraction (XRD)*

Graphite, XGO, and RGO XRD patterns are in Figure 1. Pristine graphite exhibits a sharp diffraction peak at 2θ = 26.38, corresponding to a well-ordered layer structure with 0.34 nm interlayer spacing along the (002) orientation [18]. The (002) peak shifts to a lower angle at 2θ = 10.80 after chemical oxidation and exfoliation into XGO, showing an increase in d-spacing from 0.34nm to 0.82nm. Interlayer distance between sequential carbon basal planes increases due to the interaction of oxygen functional groups with water molecules in the carbon layer structure. Nonetheless, a new broad peak at 2θ = 23.50 corresponds to a 0.38 nm d-spacing along the (002) orientation. Oxygen functional groups cause a decrease in d-spacing.

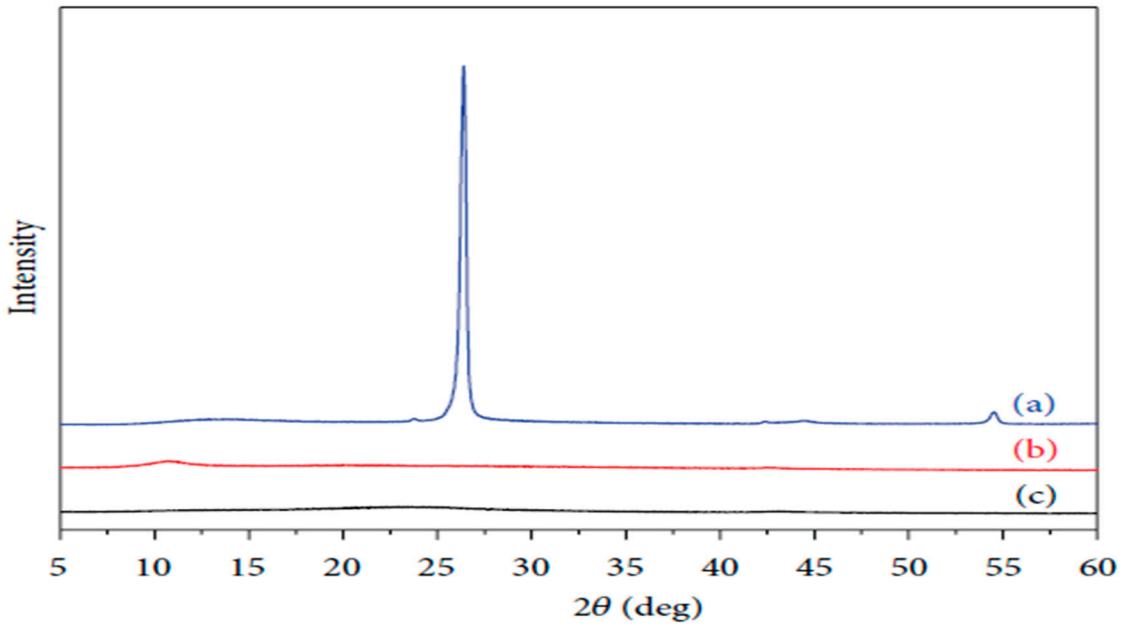


**Figure 1.** XRD patterns of (a) graphite, (b) XGO, and (c) RGO.

*5.2. Fourier Transform Infra-Red (FTIR)*

The IR spectra of both GO and rGO revealed the presence of a high absorption peak at 3352 and 3224 $cm^{-1}$, which is to the phenol or alcoholic functional group's OH-extending vibration. The absorption band at 2925 $cm^{-1}$ in rGO reveals the C-H group. The absence of the carbonyl group, the 1722 $cm^{-}$

Preprints (www.preprints.org) | NOT PEER-REVIEWED | Posted: 14 September 2023 doi:10.20944/preprints202309.0937.v1



[1] group, in rGO confirmed that GO a peak at 1351 $cm^{-1}$ in GO and 1385 $cm^{-1}$ in rGO indicates plane bending vibrations of the C-O-H bond, Indicating the introduction of oxygen groups into graphene. At 1215 $cm^{-1}$, C-O-C glycosidic linkages in the IR spectra [21]. Finally, the C-O stretching bond of C-OH is responsible for the increase in GO at 1013 $cm^{-1}$ and rGO at 1037 $cm^{-1}$. The IR data gathered showed that the absorption intensities of oxygen functional moieties were decreasing, indicating de-oxygenation and effective GO reduction. IR spectra of GO at 1215 $cm^{-1}$ and 1255 $cm^{-1}$, respectively. Finally, the C-O stretching bond of C-OH is responsible for the increase in GO at 1013 $cm^{-1}$ and rGO at 1037 $cm^{-1}$.

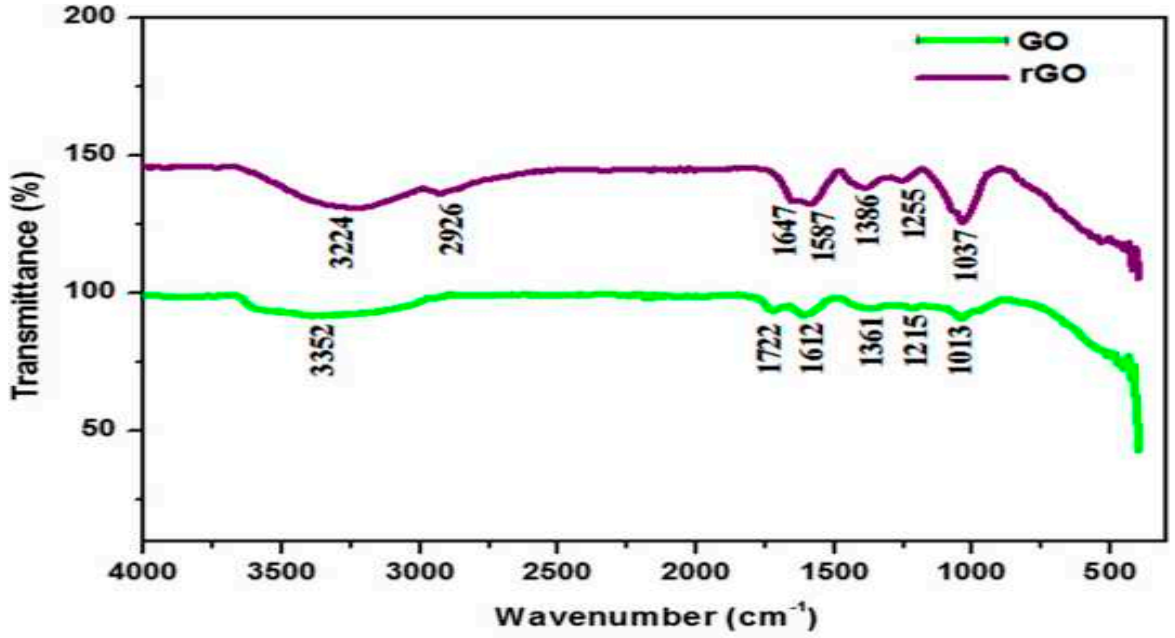


**Figure 2.** FTIR analysis of GO and rGO nanosheets.

*5.3. UV Visible Spectroscopy*

The UV-visible spectra of GO and rGO are in distilled water. It has absorption peaks at 232 nm and 300 nm due to the g-g* transition of C@C bonds and the n-g* transition of C@O bonds, respectively. This spectrum is similar to the UV-Visible Graphene Oxide made by the traditional Hummers process, and it is also identical to the GO samples described in the literature [22]. The absorption spectra of decreased GO at 260 nm showed a red shift in Figure 3. This feature aids in confirming.

Preprints (www.preprints.org) | NOT PEER-REVIEWED | Posted: 14 September 2023 doi:10.20944/preprints202309.0937.v1



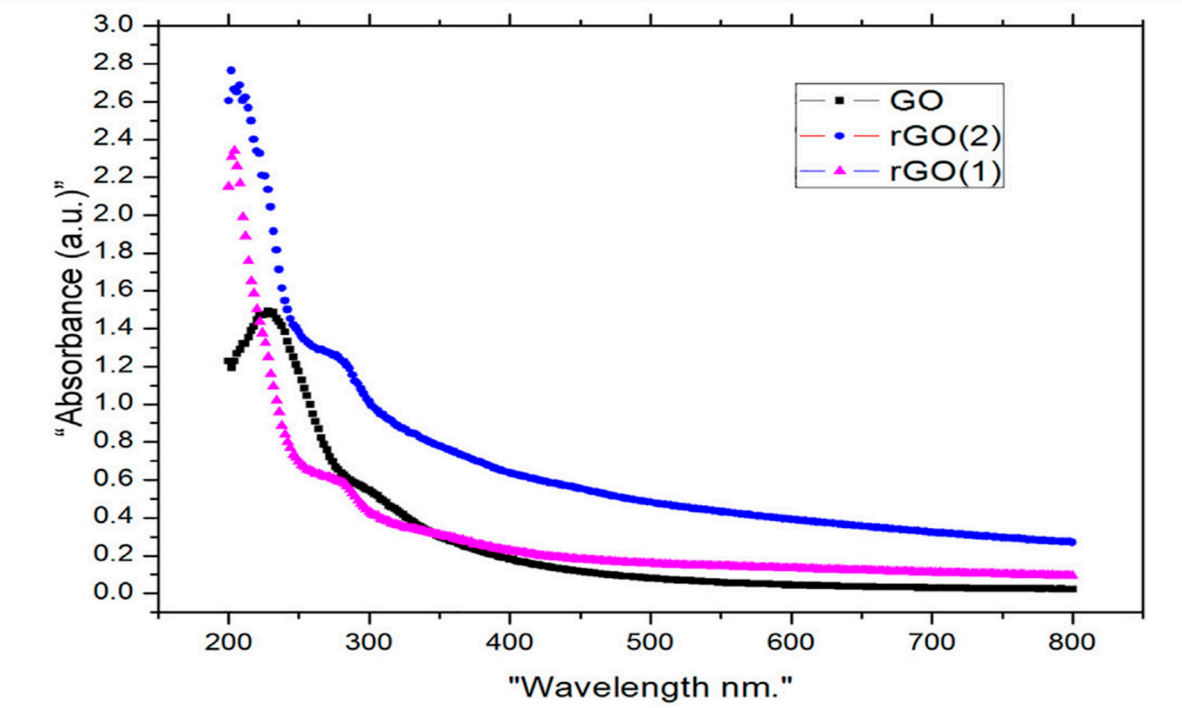


**Figure 3.** UV–Visible spectra for GO, rGO (1), and rGO (2).

*5.4. Energy Dispersive X-ray (EDX)*

When graphite is oxidized using the Hummers method (HM), the amount of carbon is reduced to 44.59%, resulting in a 2.08% rise in the atomic percentage of oxygen in the graphite (Figure 4) [22]. Other atoms involved in the process include sulfur, chlorine, calcium, potassium, and iron Figure 5. from the oxidation processes' starting chemicals and reagents.

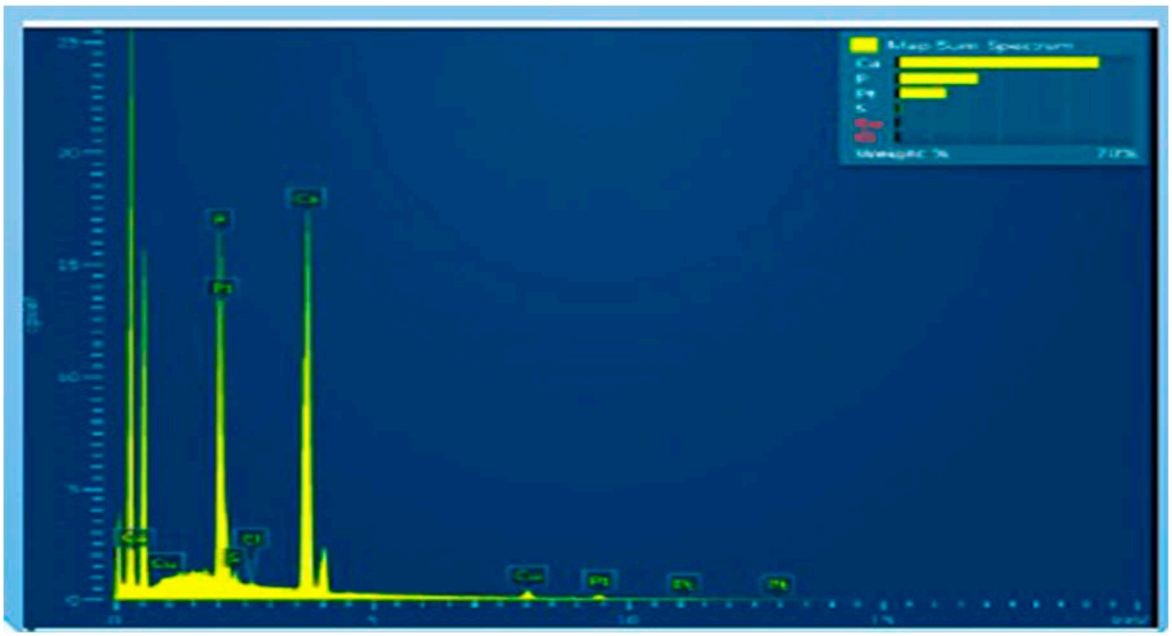

**Figure 4.** represents the EDX of (a) graphite, GO–HM, (c) GO–MHM1, and (d) GO–MHM2.

Preprints (www.preprints.org) | NOT PEER-REVIEWED | Posted: 14 September 2023 doi:10.20944/preprints202309.0937.v1



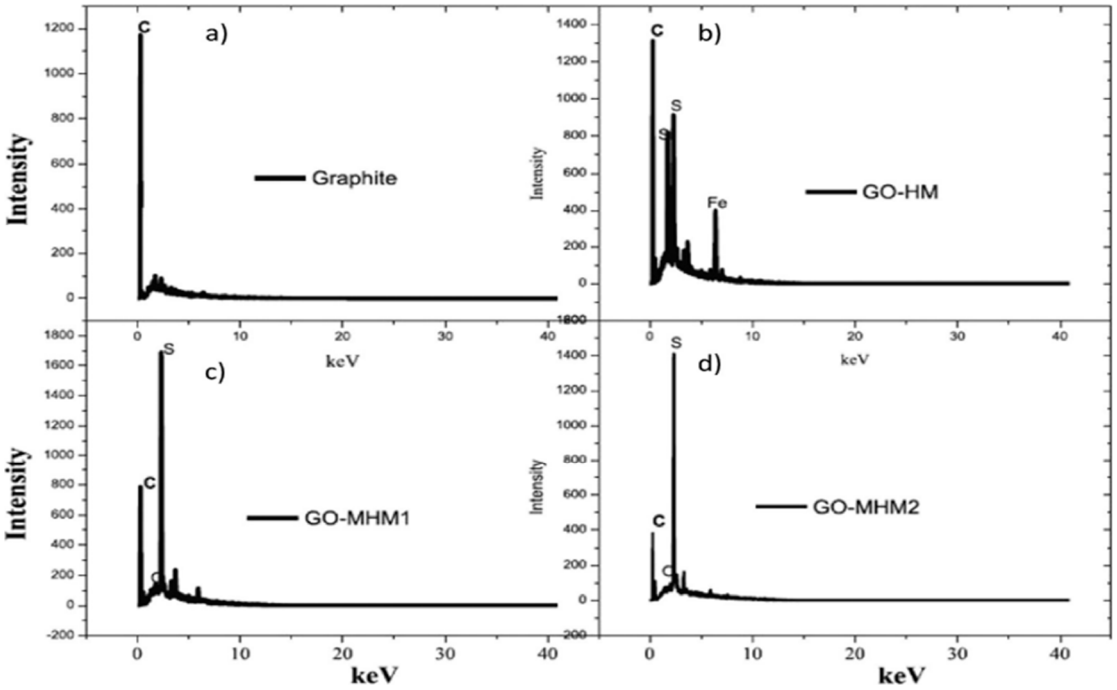


**Figure 5.** EDX of (a) graphite, (b) GO–HM, (c) GO–MHM1, and (d) GO–MHM2.

*5.5. X-ray Photoelectron Spectroscopy (XPS)*

XPS can also establish the nature of carbon and oxygen bonds in their many forms as unoxidized carbons ($sp^2$ carbon), C-O, C/O, and COOH-linked Graphene surfaces. Several GO XPS experiments validate the highest positions in various functional areas [24]. The deconvoluted C1s signal of GO, as seen in Figure 6, is composed of mainly five peaks (at room temperature) at different positions corresponding to $sp^2$ carbons in aromatic rings (284.5 eV) and C atoms bonded to hydroxyl (C-OH, 285.86 eV), epoxide (C-O-C, 286.55 eV), carbonyl (C/O, 287.5 eV), and carboxyl groups (COOH, 289.2 eV). As the temperature of GO rises, the oxygen-containing functional peaks decrease and, in some cases, disappear.

Preprints (www.preprints.org) | NOT PEER-REVIEWED | Posted: 14 September 2023 doi:10.20944/preprints202309.0937.v1



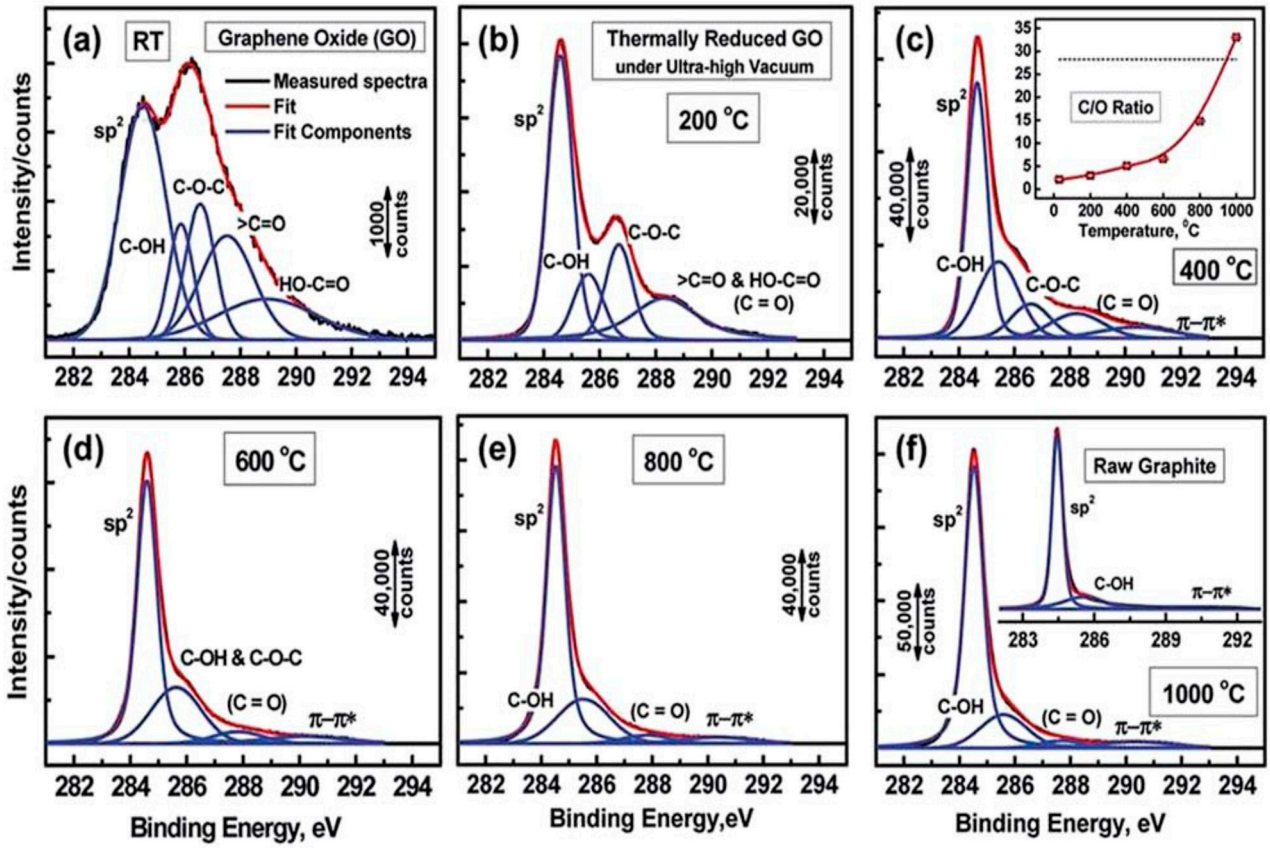


**Figure 6.** XPS spectra of GO and oxygen functionalities removal at different temperatures. Reprinted (adapted) with permission from ref.

*5.6. Raman Spectroscopy*

Raman spectroscopy is the inelastic (Raman) scattering of a molecule by monochromatic light. Then the Raman spectra of GO and RGO are shown in Figure 7. which depicts two GO and RGO vibrations between 1100 and 1700 $cm^{-1}$ [10].The D vibration band can appear at 1348.31 $cm^{-1}$ for GO and RGO, formed by a breathing mode of j-point photons with $A_1g$ symmetry. On the other hand, the G vibration band from the first-order scattering of $E_2g$ phonons by $sp^2$ carbon appears at 1594.19 $cm^{-1}$ for GO and 1586.56 $cm^{-1}$ for RGO. In addition, the ubiquitous stretched C-C bond is recemented to contribute to G band vibration.

Preprints (www.preprints.org) | NOT PEER-REVIEWED | Posted: 14 September 2023 doi:10.20944/preprints202309.0937.v1



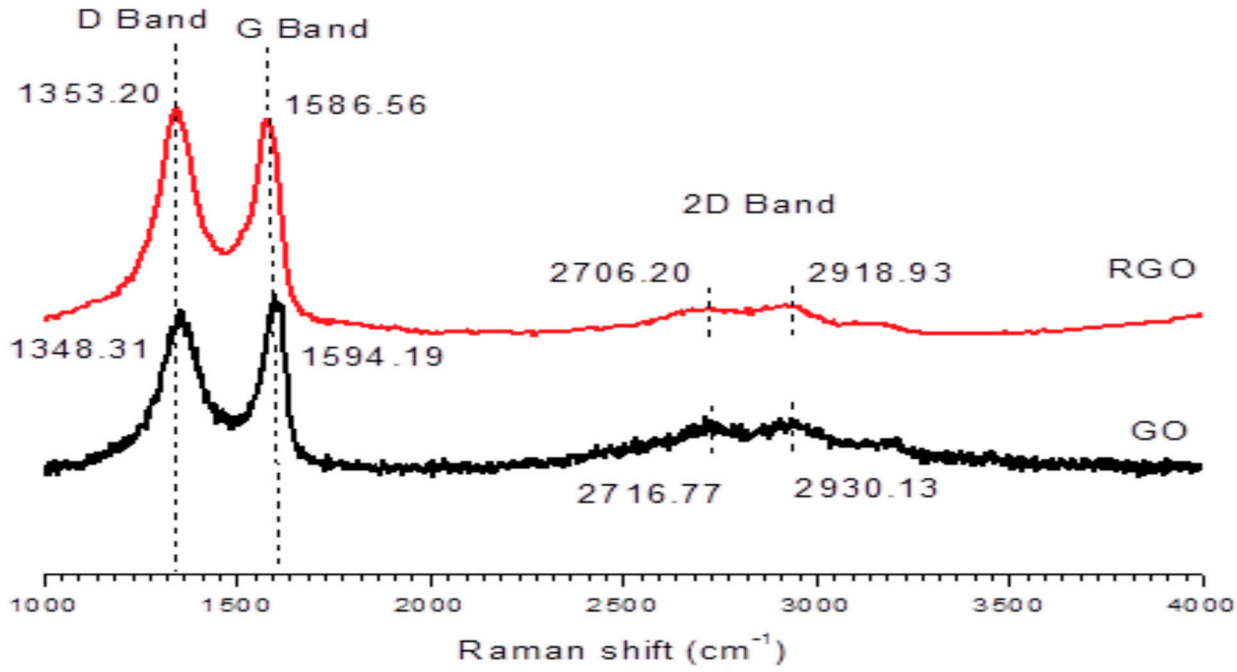


**Figure 7.** Raman spectra for GO and RGO.

*5.7. Scanning Electron Microscopy (SEM)*

SEM was used to study the morphologies of graphite, GO, and RGO samples. SEM micrographs, Figure 8 shows 10000x magnification micrographs of the graphite, GO, and RGO samples. Figure 8 (a) shows graphite under a microscope. The micrograph demonstrates that the carbon in graphite crystallized in the shape of platelets [10]. The surface of the GO, however, was coated in layered and wrinkled flakes, as seen in the SEM micrograph in Figure 8(b). Because of the presence of graphite flakes, the graphene layers completely oxidized to GO. Furthermore, Figure 8(c) depicts a micrograph of an RGO that underwent chemical reduction using hydrazine hydrate, and the RGO's surface incorporates the techniques.

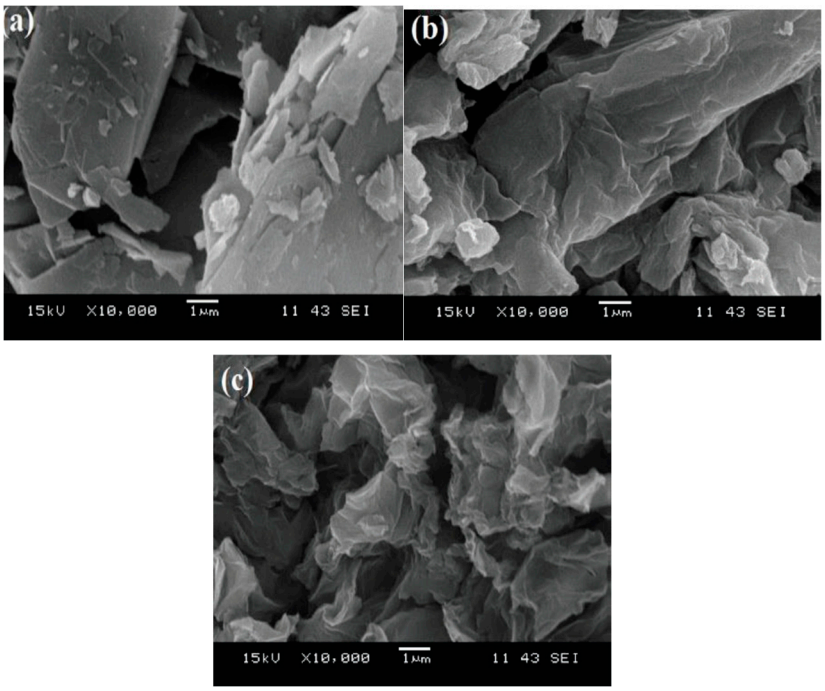


**Figure 8.** SEM micrographs of a) graphite b) GO and c) RGO.

Preprints (www.preprints.org) | NOT PEER-REVIEWED | Posted: 14 September 2023 doi:10.20944/preprints202309.0937.v1



*5.8. Transition Electron Microscope (TEM)*

TEM images to refine the morphological and structural analysis for higher resolution. Investigation reveals the spherical shape of cobalt ferrite. RGO sheets have been beneath cobalt ferrite nanoparticle particles [24]. Then RGCF nanocomposite's RGO nanosheets with smaller $CoFe_2O_4$ nanoparticles. The intimate interaction between RGO sheets and $CoFe_2O_4$ NPs prevents $CoFe_2O_4$ NP aggregation. The average particle size (Figure 9a) using the particle size distribution histogram (Figure 9d) Figure 9c's SAED pattern illustrates all the crystal lattices, demonstrating RGCF's polycrystalline nature. The spinel $CoFe_2O_4$ FCC structure can be related to the necessary lattices.

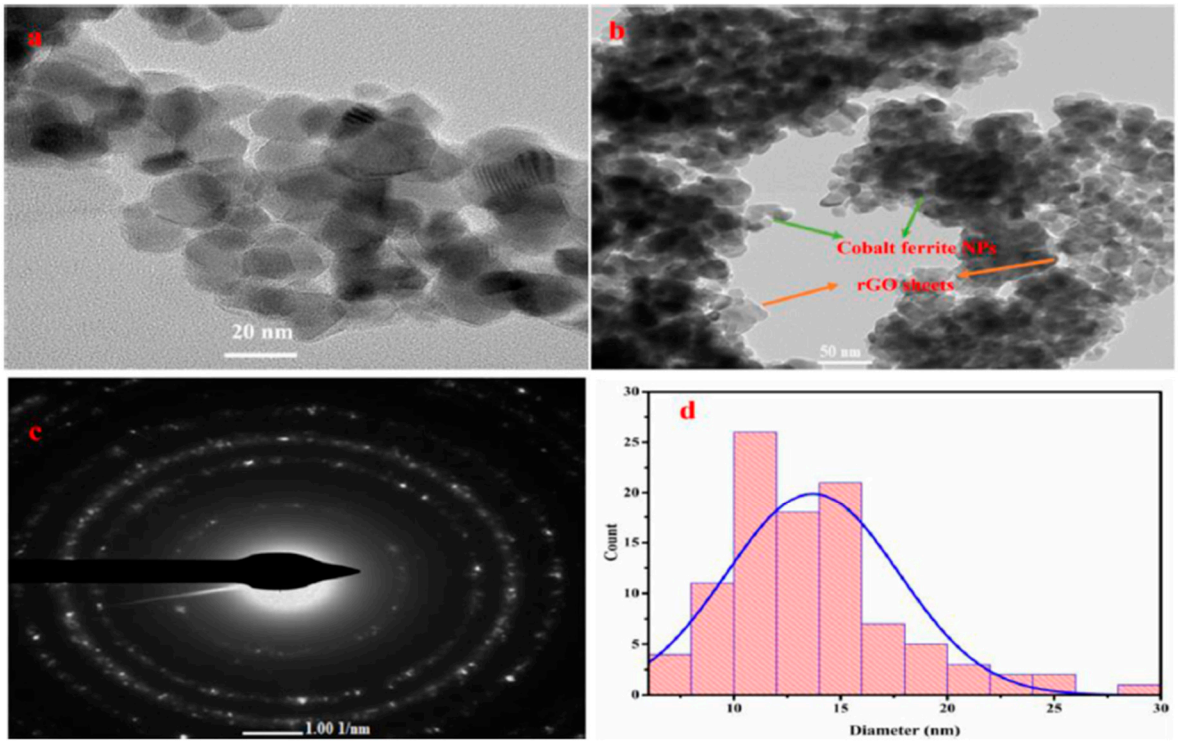


**Figure 9.** TEM images of the RGCF nanocomposite with 20 nm resolution (a), 50 nm resolution (b), SAED pattern (c), and particle size distribution (d).

*5.9. Vibrating Sample Magnetometer (VSM)*

A VSM analysis of magnetic moment plots as a function of an applied magnetic field is shown in Figure 10(a). The estimated magnetization and coercive field of $Fe_3O_4$ nanoparticles are 68.97 emu/g. As a result, they are superparamagnetic, and their behavior is consistent when placed in an external magnetic field, as seen in Figure 10(b). The coercive field and predicted magnetization values for the RGO-iron oxide nanocomposite were lowered to 47.36 emu/g and 13.43 gauss, respectively [25]. Magnetic decrease caused by magnetic nanoparticles into non-magnetic RGO to create hybrid materials. The VSM results reveal that the generated nanocomposite has good magnetic characteristics for magnetic separation in catalytic applications.

Preprints (www.preprints.org) | NOT PEER-REVIEWED | Posted: 14 September 2023 doi:10.20944/preprints202309.0937.v1



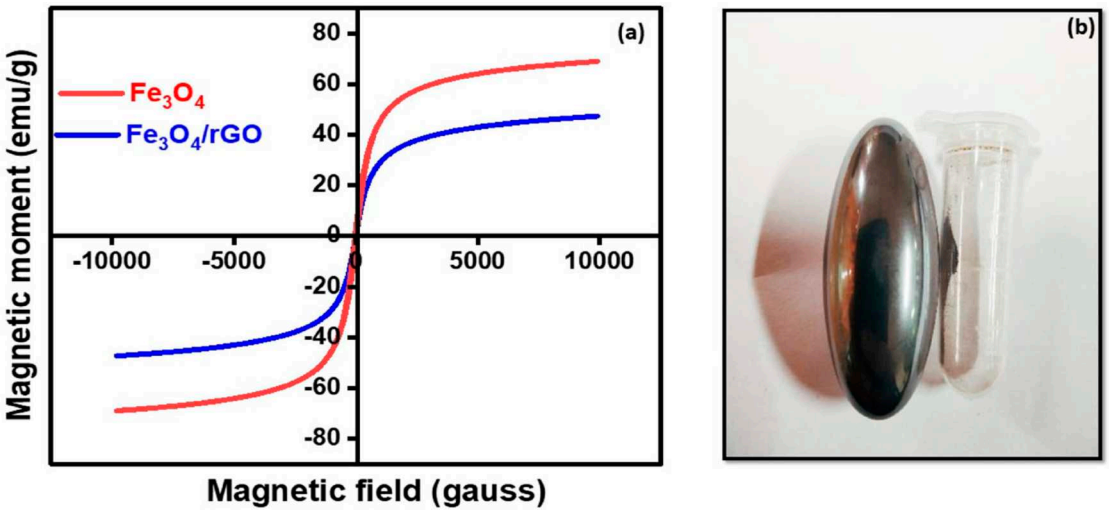


**Figure 10.** (a) Magnetic hysteresis loop for $Fe_3O_4$ NPs and $Fe_3O_4$/RGO nanocomposite. (b) The synthesized nanocomposite shows in magnetic nature when placed in an external magnetic field.

*5.10. Thermogravimetric Analysis*

The thermal removal of certain oxide groups from GO and rGO in the 50–600°C temperature range causes rGO to lose 19% more weight than GO (65%) at 600°C. rGO is more stable than GO in terms of mass at a constant temperature [26]. The weight loss of rGO (4%) and GO (5%) is due to the evaporation of adsorbed solvent molecules below 100 °C. The second period is when weight loss (27%) occurs. The weight drop (27%) is due to less stable oxides such as $H_2O$, $CO_2$, and CO gases, which produce GO. However, only 5–8% weight loss of rGO was observed from 100 to 300°C and > 300°C, respectively, in Figure 11. The elimination of more stable oxides, such as carboxyl groups, and the slow rate of weight loss were observed at temperatures above 300 °C in both samples.

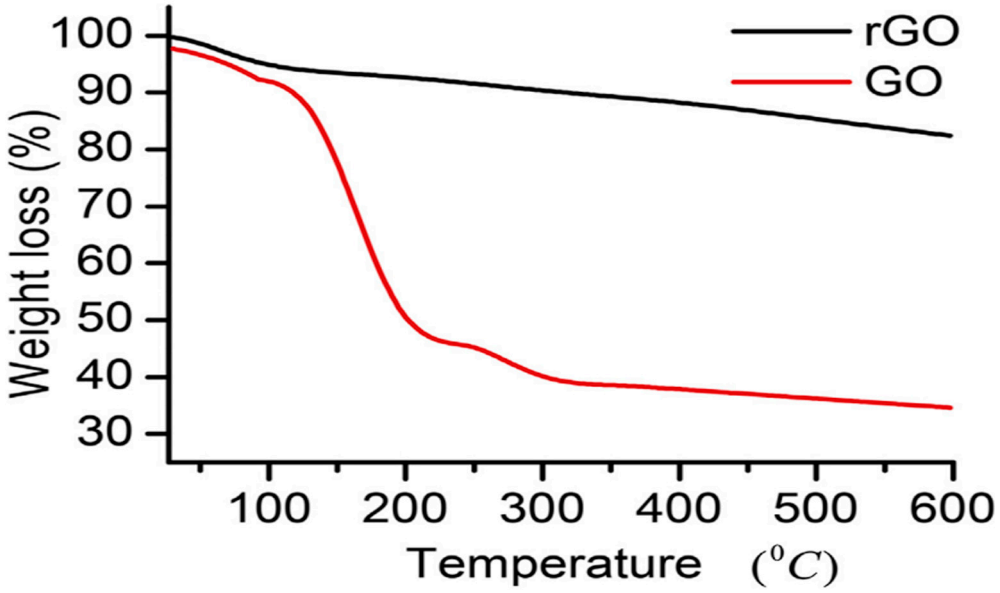


**Figure 11.** TGA for GO and RGO.

 doi:10.20944/preprints202309.0937.v1



## 6. Applications

### *6.1. Solar Cell Applications of Organic Photovoltaic*

The photovoltaic activity was produced by the interaction between patterned n-Si and GO. It operated on the p-n junction theory, where p-type GO and n-type silicon form a junction. The cell's exposure area was 0.64 $cm_2$. Voltage-based reduction uses the gold stripes on either side of the GO layer as electrodes [27]. The reduction potentials are 5 to 15 V for the GO. The photovoltaic uses the gold film deposited between GO and $SiO_2$. The solar cell's FF did not change, and the open-circuit voltage was constant at 0.78 V in every situation.

### *6.2. Graphene Supercapacitor*

The supercapacitor has high volumetric capacitance and a strong power density. With the lowest internal resistance and improved capabilities, the electrodeposition method creates a porous and conductive microarchitecture in the electrode material. The fabricated device demonstrated extraordinary cycling stability and capacitance retention during charge-discharge cycles. Over a lengthy period, an environment-friendly electrochemical device with a highly secure and stable operating energy storage supercapacitor can be an ideal choice for wearable microelectronics. The supercapacitor is optimized for stability, which has enabled high volumetric capacitance and strong power density. With the lowest internal resistance and improved capabilities, the electrodeposition method creates a porous and conductive microarchitecture in the electrode material. Devices demonstrated extraordinary cycling stability and capacitance retention during charge-discharge cycles [28]. An environmentally friendly electrochemical device with a highly secure and stable-functioning energy storage supercapacitor can be an appropriate solution for wearable microelectronics for a long time. The protocol has an excellent device structure for commercial microelectronics.

### *6.3. Graphene Sensor*

LIG in electrochemical sensor electrodes allows electrolytes to contact the surfaces of LIG electrodes, improving electron transport. Because of its many defects and exposed edge planes, LIG has more active sites and catalytic activity for redox processes, making it an attractive material for high-performance electrochemical sensors. Pure LIG, as a catalytic material, can detect biomolecules such as uric acid (UA), tyrosine (Tyr), ascorbic acid (AA), and dopamine (DA). Furthermore, LIG surface modification may boost electrochemical reactivity and broaden the types of detectable chemicals. Glucose, hydrogen peroxide, oxygen, and methane are detected using metal nanoparticles and LIG electrodes [29]. LIG-containing enzymes, aptamers, antibodies, and molecularly imprinted polymers significantly improved electrochemical sensor responsiveness and selectivity to target molecules like urea, pathogens, and antibiotics. The high electrochemical conductivity, substantial effective surface area, and high sensing performance of the hydrazine sensor are due to the composite, as sensitivity, stability, repeatability, and selectivity for cations and anions and the hydrazine sensor performed well [30]. As a result, the devised approach has potential applications for environmental water monitoring using the proposed hydrazine sensor.

Glucose monitors Glucose monitoring is critical in many fields, including clinical diagnosis, biotechnology, and the food industry [42]. To minimize diabetic emergencies, it is critical to create fast, accurate, and stable glucose detection methods, as well as frequent testing of physiological blood glucose levels. The sensor was employed for the detection of glucose in human urine samples and some chosen samples from food industries using enzymatic and non-enzymatic electrochemical methods. The proposed sensor's practical use agrees with the spectrophotometric approach. utilized in hospitals, and the glucose label value supplied by the food sector. Electrochemical immunosensor platforms for antigen and antibody detection. The detection results for both immunosensors were highly correlated [43]. From prehistoric times to the present, humanity has been plagued by a slew of viral infections. Several infectious viruses have caused global outbreaks, including influenza, Middle East respiratory syndrome coronavirus, and severe acute respiratory syndrome coronavirus. An

 doi:10.20944/preprints202309.0937.v1



accurate, quick, and sensitive diagnostic platform is one of the most important preventive strategies. This can be a helpful tool for combating pandemics and epidemics, as well as for early disease identification in areas where high-throughput approaches are required for a large population.

*6.4. Graphene Battery*

The graphene cathode is the periodic intercalation process that generates more surface vacancies to permit capacitive charge storage and, as a result, increases cathode capacity during cycling. Because of the bigger intercalant size and stress on the graphene layers during the intercalation process in Et-1.5, there was more severe cathode exfoliation than in the Emi-1.3 electrolyte [31]. At low intercalation voltages, cation co-intercalation, the co-intercalation method, and the concomitant exfoliation effect allow the Graphene battery to have an ultrahigh cathode capacity of over 150 mAh $g^{-1}$ while compromising cycle life and voltage plateaus.

*6.5. Hydro Voltaic Generators*

The droplet-based electricity generator, directly generated power, has good durability with consistent voltage output and can attain good cycling. Less wettability causes a larger output voltage, which bridges the velocity and droplet separation much more quickly. The transferred graphene device exhibits considerable voltage degradation in the long-term test because of the decreased water contact angle caused by inevitable damage and polymeric contamination during the transfer [32]. These findings demonstrate the strength of transfer-free graphene.

*6.6. Graphene in OLED Screen*

We have all witnessed significant advances in display technology over the last few years. A high contrast ratio, outstanding color quality, high brightness, acceptable brightness, size, and a completely black back are indicators of a good display. OLED has proven to be the solution to these requirements. Indium Tin oxide (ITO) is still mainly used in touch panel design. Advanced nanowires and nanoribbons for connectivity, using Graphene instead of Indium Tin oxide (ITO), solve this problem. Graphene is a thin layer with very high transparency and low sheet resistance. With its excellent mechanical strength and chemical compatibility, the use of graphene as a transparent conductive electrode is deemed the future of displays. With other transparent conductive electrodes, graphene transparency and ultra-thinness prevent light confinement, were is an outstanding property of graphene. The latest smartphone touchscreens we use have transparent indium tin oxide electrodes. The strength and flexibility of graphene make flexible screens attractive to manufacturers. A single layer of graphene can now transmit more than 97% of the incident light, far exceeding the 90° capability of ITO. Monolayer graphene has a lower conductivity than ITO, but the conductivity increases by adding layers to the material [33]. An advantage of graphene is that it does not require expensive raw materials. Carbon is abundant, making graphene affordable through efficient and effective production.

*6.7. Graphene Shielding*

Electromagnetic interference not only degrades the performance of electrical devices but also pollutes the environment and poses health hazards. Metal-based shielding materials have been used to address this issue due to their high electronic conductivity and radiation-reflecting ability. However, metal has problems such as rust, weight, and processing. corrosion-resistant, lightweight, and low-cost EMI shielding materials conducted. Conducting polymers have a remarkable ability to shield materials from electromagnetic radiation. EMI resistance of conjugated polymers. The doping of the conjugated polymers improved their electrical conductivity and radiation shielding. Electron delocalization investigation to be responsible for these polymers' increased electrical conductivity Polymer films were created by mixing an emeraldine base with dodecyl benzene sulfonic acid The electromagnetic and electrical resistance of the films were measured. Polymer films doped with acid, the thickness of which varies from 1 to 30 m [34,35]. The conductivity increased from 10 to 100 $Scm^{-1}$

as the layer thickness grew. These materials' electromagnetic interference shielding effectiveness (EMI SE) was more than 40 dB to 126 dB.

## 7. Conclusion

In this study, we looked at several synthesis and characterization methodologies. However, future research shortages and issues must be addressed and researched. It has a wide range of applications, including energy storage devices for Solar cells, Supercapacitors, LIG-based sensors, River Water sensors, Batteries, hydrovoltaic generators, OLED Screen, Polymers for Radiation Shielding, Graphene Aerogel, and it can use to make graphene.

## References


1. S. Alipour, M. Hassani, S. M. H. Hosseini, S. M. Mousavi-Khoshdel, Facile preparation of covalently functionalized graphene with 2,4-dinitrophenylhydrazine and investigation of its characteristics. RSC Adv. 2023, 13, 558.
2. Z. Hong, Z. Xin, W. Lei, B. Wang, Z. Xu, B. Ren, Y. Xiaodong, Synthesis of a Lignin-Enhanced Graphene Aerogel for Lipase Immobilization. ACS Omega. 2023, 8, 2435−2444.
3. Qian Wang, a Zhenjun Song, b Junhui Tao,a Haiqin Jin,a Sha Li,a Yuran Wang,a Xuejuan Liuc and Lin Zhang,; Interface contact and modulated electronic properties by in-plain strains in a graphene–MoS2 heterostructure. *RSC Adv.* 2023, 13, 2903.
4. **B.M. Chufa,** B.A. Gonfa, T.Y. Anshebo, G.A. Workneh, A Novel and Simplest Green Synthesis Method of Reduced Graphene Oxide Using Methanol Extracted *Vernonia Amygdalina*: Large-Scale Production. *Adv. condens. Matter Phys*. 2021, 10.
5. B. Nattha, R. Chesta, S. Chaval, Synthesis of reduced graphene oxide quantum dots from graphene oxide via hydrothermal process and their structural, luminescence and magnetic properties. *J.Taiwan Inst Chem Eng*. 2023, 142,104667.
6. *B. Cristina, P. Álvarez, P. Blanco, M. Granda, C. Blanco, R.Santamaría, L.J. Romasantab, R.Verdejo, M.A. López-Manchado, R. Menéndez,* Graphene materials with different structures prepared from the same graphite by the Hummers and Brodie methods. *Carbon*. 2013, 65, 156-164.
7. S. Sali, H.R. Mackey, A.A. Abdala, Effect of Graphene Oxide Synthesis Method on Properties and Performance of Polysulfone-Graphene Oxide Mixed Matrix Membranes. *Nanomaterials*. 2019, 9, 769.
8. M. Lojka, A. Jirickova, D. Sedmidubsky, O. Jankovsky, Fast Synthesis of Graphite Oxide via Modified Chlorate Route. *Thermophysics. 2018,* 020025, 1-6.
9. M.J. Yoo, H.B. Park, Effect of Hydrogen Peroxide on Properties of Graphene Oxide in Hummers Method. *Carbon*. 2019, 141, 515-522.
10. N. M. S. Hidayah, W.W. Liu, C.W. Lai, N. Z. Noriman, C.S. Khe, U. Hashim, H.C. Lee, Comparison on graphite, graphene oxide and reduced graphene oxide: Synthesis and Characterization. *AIP* 2017, 1892, 150005.
11. M.D.P. Lavin-Lopez, A. Romero, J. Garrido, L. Sanchez-Silva, J.L. Valverde, Influence of Different Improved Hummers Method Modifications on the Characteristics of Graphite Oxide in Order to Make a More Easily Scalable Method. *Ind. Eng. Chem. Res*. 2016, 55, 12836−12847.
12. I. Sengupta, S. Chakraborty, M. Talukdar, Thermal reduction of graphene oxide: How temperature influences purity. J. Mater. Res. 2018, 33, 4113–4122.
13. I. Sengupta, S.S. Sharat Kumar, S.K. Pal, S. Chakraborty, Characterization of structural transformation of graphene oxide to reduced graphene oxide during thermal annealing. *J. Mater. Res.,* 2020, 34, 1197–1204.

14. W. Liu, G. Speranza, Chemical Reduction of GO: Comparing Hydroiodic Acid and Sodium Borohydride Chemical Approaches by X-ray Photoelectron Spectroscopy. *Carbon*, 2022, 8, 20.
15. R. Itum, K. Sanjeev, Bamboo shoot extract as a novel and efficient reducing agent for graphene oxide and its supercapacitor application. *J Mater Sci: Mater Electron. 2023,* 11, 127.
16. R. Hidayat, S. Wahyuningsih, A.H. Ramelan, Simple synthesis of rGO (reduced graphene oxide) by thermal reduction of GO (graphene oxide). *Mater. Sci. Eng. 2020,* 858, 012009.
17. M. Ikram, A. Raza, M. Imran, A. Ul-Hamid, A. Shahbaz, S. Ali, Hydrothermal Synthesis of Silver Decorated Reduced Graphene Oxide (rGO) Nanoflakes with Effective Photocatalytic Activity for Wastewater Treatment. *Nanoscale Research Letters*. 2020, 95, 15:95.
18. V. Loryuenyong, K. Totepvimarn, P. Eimburanapravat, W. Boonchompoo, A. Buasri, Preparation and Characterization of Reduced Graphene Oxide Sheets via Water-Based Exfoliation and Reduction Methods. Adv Mater Sci Eng. 2013, 5.
19. F. Amato, A. Motta, L. Giaccari, R.D. Pasquale, F.A. Scaramuzzo, R. Zanoni, A.G. Marrani, One-pot carboxyl enrichment fosters water dispersibility of reduced graphene oxide: a combined experimental and theoretical assessment. *Nanoscale Adv. 2023*, 5, 893,
20. L. Pavko, M. Gatalo, M. Finsgar, F. Ruiz-Zepeda, K. Ehelebe, P. Kaiser, M. Geuß, T. Đukic, A.K. Surca, M. Sala, M. Bele, S. Cherevko, B. Genorio, N. Hodnik, M. Gaberscek, Graphene-Derived Carbon Support Boosts Proton Exchange Membrane Fuel Cell Catalyst Stability. *ACS Catal.* 2022, 12, 9540–9548.
21. T. Nathiya, A. Sivakumar, Green Synthesis of Reduced Graphene Oxide Nanosheets Using Leaf Extract of Lantana camara and Its In-Vitro Biological Activities. *J. Clust. Sci.* 2021, 32, 559–568.
22. S. Rattan, S. Kumar, J.K. Goswamy, Graphene oxide reduction using green chemistry. *Mater. Today: Proc.* 2020, 26, 3327-3331.
23. S. Yadav, A.P.S. Raman, H. Meena, A.G. Goswami, Bhawna, V. Kumar, P. Jain, G. Kumar, M. Sagar, D.K. Rana, I. Bahadur, P. Singh, An update on graphene oxide application and toxicity. *ACS Omega.* 2020, 7, 35387-35445.
24. L.K.J. Ting, Y. Gao, H. Wang, T. Wang, J. Sun, J. Wang, Lithium Sulfide Batteries: Addressing the Kinetic Barriers and High First Charge Overpotential. *ACS Omega.* 2022, 7, 40682-40700.
25. B. Karan, S. Jagdeep, A.S. Dhaliwal, Green synthesis and characterization of superparamagnetic nanocomposite based on reduced graphene oxide/$Fe_3O_4$ prepared using leaf extract of Azadirachta indica. *Inorg and Nano-Met Chem.* 2023, 53, 1-10.
26. G.G. Gebreegziabher, A.S. Asemahegne, D.W. Ayele, M. Dhakshnamoorthy, A. Kumar, One-step synthesis and characterization of reduced graphene oxide using chemical exfoliation method. *Mater. Today Chem. 2019*, 12, 233-239.
27. A. Singh, N. Sharma, M. Arif, R.S. Katiyar, Electrically reduced graphene oxide for photovoltaic application. *J. Mater. Res.* 34, 2019, 652–660.
28. B. Singh, R. Kaur, R. Kaur, K. Singh S. Rana A highly stable solid-state supercapacitor device based on robust layer-by-layer electrodeposited poly-(3, 4-ethylenedioxythiophene)-reduced graphene oxide–molybdenum disulfide nanocomposite electrode. *J. Energy Storage.* 2022, 56, 105926.
29. J. Zhu, X. Huang, W. Song, Physical and Chemical Sensors on the Basis of Laser-Induced Graphene: Mechanisms, Applications, and Perspectives. *ACS Nano.* 2021, 15, 18708–18741.
30. H.A. Rahman, M, Rafi, B.R. Putra, W.T. Wahyuni, Electrochemical Sensors Based on a Composite of Electrochemically Reduced Graphene Oxide and PEDOT: PSS for Hydrazine Detection. *ACS Omega*. 2023, 8, 3258–3269.

31. H. Xua, H. Chena, H. Lai, Z. Li, X. Donga, S. Cai, X. Chua, C. Gao, Capacitive charge storage enables an ultrahigh cathode capacity in aluminum-graphene battery. *J. Energy Chem.* 2020, 45, 40-44.
32. S. Jingyuan, F. Sunmiao, W. Wendong, W. Zhao, Z. Rui, L. Bingzhi, L. Li, B. Jiang, C. Haina, L. Ruojuan, W. Wang, Y. Xiaoqin, G. Wenyue , H.R. Mark, G. Wanlin, S. Jingyu, L. Zhongfan, Copper acetate-facilitated transfer-free growth of high-quality graphene for hydrovoltaic generators. *Natl Sci Rev*, 2022, 9, 1-9.
33. S. Reena, K. Ramsingh, S. Sushama, K.G. Kallol, Facile and scalable synthesis of un-doped, doped and co-doped graphene quantum dots: a comparative study on their impact for environmental applications. *RSC Adv.* 2023, 13, 701.
34. K. Ayesha, Nanocarbon Nanocomposites of Polyaniline and Pyrrole for Electromagnetic Interference Shielding: Design and Effectiveness, *Polym Plast Technol Mater*. 2022, 61, 1988-2000.
35. L.D. Yun, J.Z. Xiao, Y.W. Bian, Y.D. Qiu, Facile synthesis of polypyrrole nanoparticles with tunable conductivity for efficient electromagnetic wave absorption and shielding performance. CrystEngComm, 2022, 24.
36. A.T.Smith,A.M.Lachance,S.Zeng,B.Liu,L.Sun. Synthesis, properties, and applications of graphene oxide/reduced grapheneoxide and their nanocomposites, NMS(2019).
37. S.Singh, M.R.Hasan, P.Sharma, J.Narang, Graphene nanomaterials: The wondering material from synthesisto applications, Sens.Int.3(2022).
38. Z. Iqbal, M.S. Tanweer, M. Alam, Reduced Graphene Oxide-Modified Spinel Cobalt Ferrite Nanocomposite: Synthesis, Characterization, and Its Superior Adsorption Performance for Dyes and Heavy Metals. ACS Omega 2023, 8, 6376−6390.
39. I. Bychko, A. Abakumov, O. Didenko, M. Chen, J. Tang, P. Strizhak, Differences in the structure and functionalities of graphene oxide and reduced graphene oxide obtained from graphite with various degrees of graphitization. Journal of Physics and Chemistry of Solids 164 (2022) 110614.
40. V.C. Fernandes, V.F. Domingues, M. S. Nunes, R. Matos, I. Kuźniarska-Biernacka, D.M. Fernandes, A. Guerrero-Ruiz, I.R. Ramos, C. Freire, C. Delerue-Matos, Graphene-Type Materials for the Dispersive Solid-Phase Extraction Step in the QuEChERS Method for the Extraction of Brominated Flame Retardants from Capsicum Cultivars. J. Agric. Food Chem. 2023, 71, 8, 3898–3905.
41. H. Kang, D.Y. Kim, J. Cho, Top-Down Fabrication of Luminescent Graphene Quantum Dots Using Self-Assembled Au Nanoparticles. ACS Omega 2023, 8, 5885−5892.
42. B.A. Hussein, A. Abebaw. T.B.G. Shiferac. A.M. Taddessed, A sensitive non-enzymatic electrochemical glucose sensor based on a ZnO/Co3O4/reduced graphene oxide nanocomposite. RSC Adv., 2023.
43. M.S. Abubakar, Y. Shalu, R. Pushpesh, K. Raju, K. Firoz, K. Ashok, B. Debasis, Highly Sensitive Electrochemical Immunosensor Platforms for Dual Detection of SARS-CoV-2 Antigen and Antibody-based on Gold Nanoparticle Functionalized Graphene Oxide nanocomposites. ACS Appl. Bio Mater. 2022, 5, 2421−2430.